Copyright © IFAC Modelling and Control in Biomedical Systems, Melbourne, Australia, 2003

ELSEVIER
IFAC
PUBLICATIONS
www.elsevier.com/locate/ifac

CYCLE-AVERAGED MODELS OF CARDIOVASCULAR DYNAMICS

Thomas Heldt[1], Jolie L. Chang[2], George C. Verghese[3], and Roger G. Mark[1]

[1]Harvard University – MIT Division of Health Sciences and Technology, Massachusetts Institute of Technology, USA
[2]School of Medicine, University of California, San Francisco, USA
[3]Laboratory for Electromagnetic and Electronic Systems, Massachusetts Institute of Technology, USA

Abstract: Time-varying ventricular elastance models have been used extensively in the past to simulate the pulsatile nature of cardiovascular waveforms. Frequently, however, one is interested in dynamics that occur over longer timescales in which case a detailed simulation of each cardiac contraction becomes computationally burdensome. In this paper, we apply circuit-averaging techniques to a simplified lumped-parameter model of the cardiovascular system. The resultant cycle-averaged model is linear and time invariant, and greatly reduces the computational burden. It is also amenable to systemic order reduction methods that lead to further efficiencies. Despite its simplicity, the averaged model captures the dynamics relevant to the representation of a range of cardiovascular reflex mechanisms. *Copyright © 2003 IFAC*

Keywords: Average Values, Biomedical Systems, Circuits, Model Reduction, Simulation, Transient Analysis

1. INTRODUCTION

Over the past thirty years, computational models of cardiovascular function have become abundant in both basic research and teaching, with increasingly more sophisticated models becoming available at any biological size and time scale. At the system level, time-varying ventricular elastance models have proven to be useful representations of the right and left heart [see, e.g., (Sunagawa and Sagawa, 1982)], that, when coupled to appropriate models of the peripheral systemic and pulmonary circulations, allow for simulation of realistic pulsatile pressure and flow waveforms. Frequently, however, one is not interested in an instantaneous value of a particular variable or the details of a specific waveform but rather in the system's average response to perturbations in its parameters. This response typically occurs over time scales that are large compared to the dynamics of cardiac contraction. In these cases, a cycle-averaged model, which tracks cycle-to-cycle (i.e. intercycle) dynamics rather than intracycle dynamics, seems desirable for several reasons. First, by ignoring the fine intracycle structure of each waveform, one can expect to reduce computational time significantly. Second, one can anticipate that analysis of the dynamics of interest simplifies if the model structure is reduced sufficiently. Third, it is typically the time-averages and not instantaneous values of key state variables that are regulated through the feedback control embodied in cardiovascular reflex mechanisms.

The goal of this paper, which builds on (Chang, 2002), is to study a simplified lumped-parameter hemodynamic model and to derive a cycle-averaged version of it by applying circuit-averaging techniques from the power electronics literature (Verghese, 1996). The process of cycle-averaging preserves the state-space description of the model. Furthermore, the resulting model structure turns out to be linear and time-invariant (LTI), which allows for further insight into and simplification of the model structure.

2. PULSATILE MODEL

We implemented a simplified version of a lumped-parameter representation of a previously published closed-loop pulsatile hemodynamic model (Heldt et al., 2002). The simplified model is still rich enough to represent the essential time-varying dynamics of

the pulsatile model and to serve as a sufficient testbed for our development of an averaging methodology. As shown in Figure 1, the model is in circuit form, and consists of three segments, representing a cardiac, an arterial, and a venous compartment, respectively. The pumping action of the heart is represented by a single ventricular time-varying compliance, $C(t)$ [the inverse of a time-varying elastance, $E(t)$, i.e. $C(t) = 1/E(t)$], which cycles with period T between a diastolic value C_D of duration T_D, and a systolic value C_S of duration T_S, as shown in Figure 2. We assume T_S / T_D = ½ for convenience. Voltages in this circuit analog represent pressures, and currents represent blood flows.

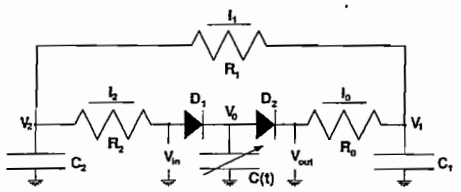

Fig. 1. Pulsatile model. $C(t)$ is a time-varying compliance; V_{in} and V_{out} are defined here for future reference (see Section 3.2); the voltages V_0, V_1, V_2 represent cardiac, arterial, and venous pressures, respectively.

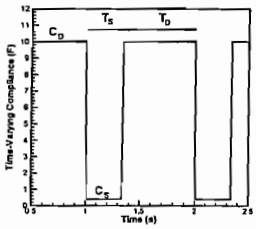

Fig. 2. Time-varying compliance waveform.

The arterial and venous compartments are characterised by constant resistances and compliances. The system is thus described by a set of three coupled linear differential equations:

$$\begin{aligned} \frac{d}{dt}\left[C(t)\cdot V_0(t)\right] &= \left[i_2(t)-i_0(t)\right] \\ \frac{d}{dt}V_1(t) &= \frac{1}{C_1}\left[i_0(t)-i_1(t)\right] \\ \frac{d}{dt}V_2(t) &= \frac{1}{C_2}\left[i_1(t)-i_2(t)\right] \end{aligned} \qquad (1)$$

The currents can be expressed using the constitutive relations for the resistors:

$$\begin{aligned} i_0(t) &= \frac{1}{R_0}\left[V_0(t)-V_1(t)\right] \\ i_1(t) &= \frac{1}{R_1}\left[V_1(t)-V_2(t)\right] \\ i_2(t) &= \frac{1}{R_2}\left[V_2(t)-V_0(t)\right] \end{aligned} \qquad (2)$$

Table 1 shows the parameter assignments and initial conditions for the pulsatile model.

Table 1. Parameter assignments and initial conditions for the pulsatile model

Compartment:	0	1	2
R (Ω)	0.01	1.0	0.03
C (F)	0.4 – 10.0	2.0	100.0
$V_{initial}$ (V)	7.0	56.0	9.0

Figure 3 shows the voltage waveforms generated with the pulsatile model described above. It should be pointed out that the spikes in the voltage V_0 are non-physiologic and not seen if a more realistic time-varying compliance waveform is used [see, e.g., Heldt et al., 2002)]. Figure 4 shows the transient response of the voltage waveforms to a step in the resistance R_1 at time t=5s and demonstrates that changes in the cycle-to-cycle dynamics occur over timescales that are large compared to the timescale of intracycle dynamics.

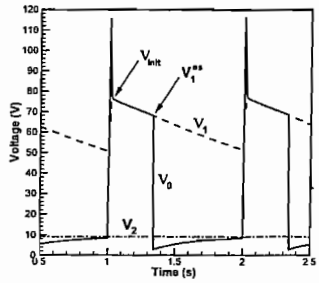

Fig. 3. Voltage waveforms generated using the pulsatile model. V_1^{α} and V_{init} are defined here for future reference.

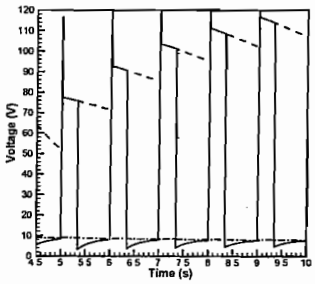

Fig. 4. Transient response of pulsatile waveforms to a step change in the resistance R_1 from 1.0 Ω to 5.0 Ω at time t=5s.

3. DEVELOPING A CYCLE-AVERAGED MODEL

In developing a cycle-averaged version of the simplified cardiovascular model, we make use of the definition of the symmetric time-average of a periodic waveform V over a period T:

$$\langle V(t)\rangle = \frac{1}{T}\int_{t-T/2}^{t+T/2} V(\tau)\,d\tau \qquad (2)$$

An important property of this definition is that the derivative of the time-averaged waveform equals the time-average of its derivative, i.e.

$$\left\langle \frac{d}{dt} V(t) \right\rangle = \frac{d}{dt} \langle V(t) \rangle \quad (3)$$

When averaging constraint equations for terminal voltages, currents, and charges of linear and time-invariant components of the circuit, such as Ohm's law for a linear resistor, one can easily verify that the time-averaged voltages, currents, and charges obey the same constraints as their instantaneous counterparts. Our attention in finding a cycle-averaged description of the pulsatile model therefore focuses on finding a cycle-averaged description of the elements that give rise to the nonlinear and time-varying nature of the circuit, namely the diodes and the time-varying elastance.

3.1 Replacing the time-varying elastance

The cycle-averaged voltage across the central capacitor is given by

$$\langle V(t) \rangle = \langle E(t) \cdot Q(t) \rangle \quad (4)$$

If the instantaneous charge $Q(t)$ were of low ripple[1], one could approximate the average of the product on the right hand side by the product of the averages. In the pulsatile model described above, however, $Q(t)$ has a relative peak-to-peak ripple of approximately 100%, which is certainly not low ripple. We therefore expanded both $E(t)$ and $Q(t)$ in a Fourier series to first order:

$$\begin{aligned} E(t) &\approx E_0 + E_1 \cdot \cos\left(\frac{2\pi}{T}\right) + E_2 \cdot \sin\left(\frac{2\pi}{T}\right) \\ Q(t) &\approx Q_0 + Q_1 \cdot \cos\left(\frac{2\pi}{T}\right) + Q_2 \cdot \sin\left(\frac{2\pi}{T}\right) \end{aligned} \quad (5)$$

The right-hand side of equation (4) can now be equated to

$$\langle E(t) \cdot Q(t) \rangle \approx E_0 Q_0 + \tfrac{1}{2}\left(E_1 Q_1 + E_2 Q_2\right) \quad (6)$$

E_0 and Q_0 are equivalent to $\langle E(t) \rangle$ and $\langle Q(t) \rangle$, respectively. Since, for now, $E(t)$ is strictly periodic, E_0, E_1, and E_2 are constant. Furthermore, Q_1 and Q_2 can assumed to be constant over the cycle period T. The second term on the right-hand side of equation (6) therefore represents an offset voltage, V_{offset}, that is approximately constant over the averaging interval. Equation (4) therefore equates to

$$\langle V(t) \rangle \approx \langle E \rangle \cdot \langle Q(t) \rangle + V_{offset} \quad (7)$$

The time-averaged rate of change of the charge on the central capacitor, i.e. the current flowing into or out of the capacitor, can now be evaluated using equation (7):

$$\begin{aligned} \langle i(t) \rangle = \frac{d}{dt} \langle Q(t) \rangle &\approx \frac{d}{dt}\left(\frac{\langle V(t) \rangle - V_{offset}}{\langle E \rangle} \right) \\ &= \frac{1}{\langle E \rangle} \cdot \frac{d}{dt} \langle V(t) \rangle \end{aligned} \quad (8)$$

The final equality in (8) follows from the constancy of $\langle E \rangle$ and V_{offset}. Using the definitions in Figure 2, $\langle E \rangle$ is given by

$$\langle E \rangle = \frac{T_S}{T C_S} + \frac{T_D}{T C_D} \quad (9)$$

The time-varying elastance introduced in Section 2 can therefore be replaced using a constant capacitor with capacitance $C_{eff} = 1/\langle E \rangle$ and constant offset voltage V_{offset}.

3.2 Replacing the diodes D_1 and D_2

To deal with the diodes D_1 and D_2, we introduce a switching function $q(t)$ that is 1 when the diode D_1 is conducting and 0 when D_1 is non-conducting. The square-wave nature of the time-varying compliance waveform allows for two simplifications: (1) $q(t)$=1 throughout T_D and $q(t)$=0 throughout T_S and (2) a switching function for D_2 is given by $[1-q(t)]$, i.e. D_2 is conducting when D_1 is not and vice-versa. To study the currents through the diodes, it will be convenient to introduce the following voltages (also see Figure 1):

$$\begin{aligned} V_{out} &= [1-q(t)] \cdot V_0(t) + q(t) \cdot V_1(t) \\ V_{in} &= q(t) \cdot V_0(t) + [1-q(t)] \cdot V_2(t) \end{aligned} \quad (10)$$

The time averages of the currents i_0 and i_2 can now be represented using the switching function q(t):

$$\begin{aligned} \langle i_0(t) \rangle &= \frac{1}{R_0}\left(\langle V_{out} \rangle - \langle V_1 \rangle \right) \\ &= \frac{1}{R_0}\left(\langle V_0(t) \rangle - \langle q(t) \cdot V_0(t) \rangle \right) + \\ &\quad + \frac{1}{R_0}\left(\langle q(t) \cdot V_1(t) \rangle - \langle V_1(t) \rangle \right) \end{aligned} \quad (11)$$

$$\begin{aligned} \langle i_2(t) \rangle &= \frac{1}{R_2}\left(\langle V_2 \rangle - \langle V_{in} \rangle \right) \\ &= \frac{1}{R_2}\left(\langle q(t) \cdot V_2(t) \rangle - \langle q(t) \cdot V_0(t) \rangle \right) \end{aligned} \quad (12)$$

The remainder of this sub-section will be devoted to finding appropriate approximations to the terms in equations (11) and (12) that are averages of a product of the switching function with one of the voltage waveforms. We seek approximations invoking combinations of averaged waveforms to replace the averages of combinations of waveforms.

The diastolic venous waveform: $\langle q(t) \cdot V_2(t) \rangle$ represents the cycle-averaged diastolic venous waveform. Owing to the large value of C_2, V_2 is approximately constant around the value $\langle V_2 \rangle$ as can be seen from Figure 3. It is therefore appropriate to approximate the diastolic venous waveform by

$$\begin{aligned} \langle q(t) \cdot V_2(t) \rangle &\approx \langle q(t) \rangle \cdot \langle V_2(t) \rangle = \\ &= \frac{T_D}{T} \cdot \langle V_2(t) \rangle \end{aligned} \quad (13)$$

The diastolic cardiac waveform: $q(t) \cdot V_0(t)$ represents the cardiac waveform during diastole. The time course of this can be expressed as follows

$$V_0^d(t) = V_0^{bd} + \left(V_2 - V_0^{bd} \right) \cdot \left(1 - \exp\left[-\frac{t}{C_D R_2} \right] \right) \quad (14)$$

[1] The relative peak-to-peak ripple of a waveform V is $V_{pp} = (V_{max} - V_{min})/\langle V \rangle$.

By invoking continuity of charge (blood volume), the cardiac voltage at the beginning of diastole, V_0^{bd}, can be expressed in terms of the arterial end-systolic voltage, V_1^{es}, according to

$$V_0^{bd} = \frac{C_S}{C_D} \cdot V_1^{es} \tag{15}$$

Inserting equation (15) into equation (14) and applying the cycle-averaging operation results in a cycle-averaged expression for the diastolic cardiac waveform:

$$\langle q(t) \cdot V_0(t) \rangle = \frac{R_2}{T}\left(C_D \langle V_2 \rangle - C_S V_1^{es}\right) \cdot \left(\exp\left[-\frac{T_D}{C_D R_2}\right] - 1\right) + \frac{T_D}{T}\langle V_2 \rangle \tag{16}$$

Equation (16) necessitates finding an expression for $\langle V_1^{es} \rangle$ in terms of the other cycle-averaged voltages.

End-systolic arterial voltage: To find an expression for the end-systolic arterial voltage, V_1^{es}, we make a straight-line approximation of the arterial voltage waveform $V_1(t)$ with a slope of $-\frac{V_{init}}{R_1 C_1}$, as suggested by Figure 3. Under this assumption, it can be easily verified that V_1^{es} is given by

$$V_1^{es} = \langle V_1 \rangle \cdot \frac{2R_1C_1 - 2T_S}{2R_1C_1 - T} \tag{17}$$

The diastolic arterial voltage: The diastolic portion of the arterial waveform can be approximated by

$$V_1^d(t) = \left(V_1^{es} - V_2\right) \cdot \exp\left(\frac{t}{R_1 C_1}\right) + V_2 \tag{18}$$

so that the cycle-averaged diastolic arterial waveform is given by

$$\langle q(t) \cdot V_1(t) \rangle = \frac{T_D}{T}\langle V_2 \rangle + \frac{R_1 C_1}{T}\left(V_1^{es} - \langle V_2 \rangle\right) \cdot \left(1 - \exp\left[\frac{T_D}{R_1 C_1}\right]\right) \tag{19}$$

into which (17) can be substituted.

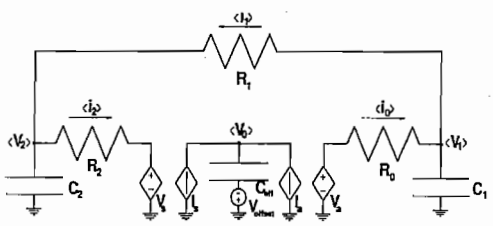

Fig. 5. Circuit representation of the cycle-averaged model. V_s, V_a, I_s, and I_a are voltage and current sources, respectively, that depend on the cycle averaged voltages in the circuit.

3.3 Model structure and initial conditions

Combining the results of the last four sub-sections with equations (1), (8), (11), and (12), it emerges that the resultant cycle-averaged model can be represented by the LTI circuit model in Figure 5, and equivalently by a state-space model of the form

$$\frac{d}{dt}\begin{bmatrix}\langle V_0(t)\rangle \\ \langle V_1(t)\rangle \\ \langle V_2(t)\rangle\end{bmatrix} = \begin{bmatrix} & A & \end{bmatrix} \cdot \begin{bmatrix}\langle V_0(t)\rangle \\ \langle V_1(t)\rangle \\ \langle V_2(t)\rangle\end{bmatrix} \tag{20}$$

An eigenvalue decomposition of A reveals the following eigenvalues $[\lambda_1, \lambda_2, \lambda_3] = [-109.02, -0.68, 0\,0]$. The negative reciprocals of the three eigenvalues of A are the time constants of the exponentials that govern the response of the model to initial conditions. The eigenvalue λ_1 is irrelevant to our simulations as it corresponds to a time constant much smaller than our averaging interval T. The second eigenvalue corresponds to a time constant of approximately 1.49s. The final eigenvalue, $\lambda_3 = 0.0$, with its corresponding eigenvector E_3 indicates that a non-zero steady-state solution exists. In fact, after initial transients due to λ_1 and λ_2 have subsided, the system will settle in a new steady-state S proportional to E_3

$$S = \gamma \cdot E_3 \tag{21}$$

where γ is determined by the total charge in the system according to the constraint

$$Q_{total} = \left[C_{eff},\ C_1,\ C_2\right]\begin{bmatrix}\gamma \cdot E_{31} - V_{offset} \\ \gamma \cdot E_{32} \\ \gamma \cdot E_{33}\end{bmatrix} \tag{22}$$

We can determine γ by requiring that the total charge in the cycle-averaged model equal the total charge in the pulsatile model. The state S then becomes a natural choice for the initial conditions of the cycle-averaged model. Using the waveforms generated by the pulsatile model, the offset pressure can be computed to $V_{offset} = -14.51$. The total charge of the pulsatile model is 1082C, which leads to $\gamma = 70.69$. Thus the initial condition for the cycle-averaged model is given by $S' = [27.84, 64.34, 9.06]$.

4. COMPARISON OF SIMULATIONS

To evaluate the performance of the cycle-averaged model we will compare its simulation results and simulation time to that of the pulsatile model.

4.1 Comparison of steady-state numerics

In Table 2, the steady-state responses of the cycle-averaged model (CAM) and the pulsatile model (PM) are compared. All but two of the steady-state values show a negligible discrepancy between the cycle-averaged and the pulsatile model. The remaining two variables are not independent, and an improvement in V_0 will certainly lead to an improvement in q_0. One could tune the offset voltage V_{offset} in the cycle-averaged model to reduce the discrepancy of V_0 between the cycle-averaged and the pulsatile model.

Table 2. Comparison of steady-state simulation results

Variable	PM	CAM	Rel. Error
V_0 (V)	29.23	27.85	-4.7 %
V_1 (V)	64.07	64.36	0.5 %
V_2 (V)	9.01	9.06	0.6 %
i_0 (A)	55.06	55.30	0.4 %
i_1 (A)	55.06	55.30	0.4 %
i_2 (A)	55.09	55.30	0.4 %
q_0 (C)	53.03	47.06	-11.26 %
q_1 (C)	128.14	128.72	0.5 %
q_2 (C)	900.83	906.22	0.6 %

4.2 Comparison of dynamic responses

To compare the responses of the two models to changes in their parameters, we chose to (1) perturb the arteriolar resistance R_1, and (2) the cycle period T. Both parameters play important roles in cardiovascular homeostasis through feedback regulation, and both have the capacity to change by a factor of 2 over short periods of time. Figure 6 shows the beat-by-beat averaged response of the pulsatile model (solid line) and the response of the cycle-averaged model (dashed line) to a change in R_1. At time t=15s, the resistance is ramped from R_1=1.0 Ω to R_1=2.0 Ω over a period of 2 s. At time t=45 s, this process is reversed. Figure 7 shows the transient dynamics of both models when the cycle period is changed in a step from T=1.0 s to T=0.5 s. The step is again reversed at t=45 s. Both transient simulations show that the time constants of the system-level response are preserved well by the cycle-averaged model. The main discrepancy between the simulation outputs of the two models is the static offset in the steady state value of V_0.

4.3 Computational efficiency

Both the pulsatile and the cycle-averaged model were implemented in the C programming language using a LINUX operating system on a PC (AMD Athlon 1.2 GHz processor). A standard fourth-order Runge-Kutta integrator was used to solve the differential equations numerically.

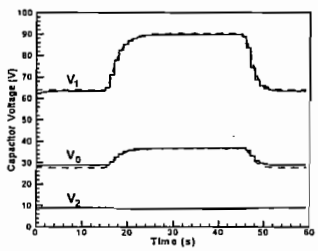

Fig. 6. Transient response to changes in R_1. CAM: dashed line; PM: solid line.

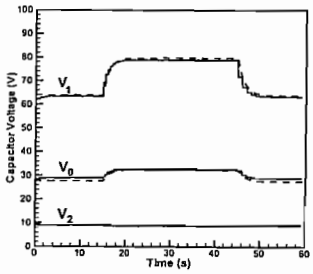

Fig. 7. Transient responses to changes in T. CAM: dashed lines; PM: solid lines.

Due to square-wave nature of the time-varying compliance waveform, a step size of 10^{-6} s was used for the pulsatile model. In Table 3, we present the steady state voltages of the pulsatile model and of the cycle-averaged model for three different step sizes. The source codes were compiled using the *–pg* option of the gcc compiler. Each program was run for 10,000 s and LINUX's Gprof utility was used to assess the CPU time. The CPU times given in the table below are averages of five separate runs for each program.

Table 3. Computational efficiency vs. simulation accuracy

Variable	PM	CAM		
step size (s)	10^{-6}	10^{-4}	10^{-3}	10^{-2}
V_0 (V)	29.23	27.85	27.85	27.85
V_1 (V)	64.07	64.36	64.36	64.36
V_2 (V)	9.01	9.06	9.06	9.06
CPU time (s)	13077.7	190.1	19.0	1.9

As can be seen from this table, the CPU time for the cycle-averaged model can be improved by a factor of 7000 over the pulsatile model without degradation of accuracy.

5. MODEL REDUCTION

As noted in Section 3.3, the cycle-averaged model has one very fast time constant $\tau_1 = -1/\lambda_1 \approx 0.009s$. As mentioned before, this time constant is much smaller than our averaging interval and is therefore irrelevant to the cycle-averaged model. Using ideas from singular perturbation theory [see, e.g., (Caliskan et al., 1999)], we can accordingly partition the cycle-averaged state- space model as follows

$$\begin{bmatrix} \dot{x}_f \\ \dot{x}_s \end{bmatrix} = \begin{bmatrix} A_1 & A_2 \\ A_3 & A_4 \end{bmatrix} \cdot \begin{bmatrix} x_f \\ x_s \end{bmatrix} \qquad (23)$$

where x_f and x_s correspond to rapidly and slowly varying signals, respectively. In our case, the structure of the matrix A in (21), suggests that x_f corresponds to $\langle V_0 \rangle$ and x_s to $[\langle V_1 \rangle, \langle V_2 \rangle]$. Since x_f is a signal with a very fast transient, $\dot{x}_f$ will be approximately zero after a short time interval.

Consequently, x_f can be written in terms of x_s following the fast transient interval:

$$x_f \approx -A_1^{-1} A_2 \cdot x_s \tag{24}$$

Substituting this in the expression for $\dot{x}_s$ yields a reduced-order cycle-averaged model, still in state space form:

$$\dot{x}_s \approx \left(A_4 - A_3 A_1^{-1} A_2 \right) \cdot x_s \tag{25}$$

In Table 4, we compare the steady-state capacitor voltages and CPU times for the largest possible time steps that the pulsatile, the cycle-averaged, and the reduced-order models permit. The CPU times are again based on 10,000s simulations, and represent the averages of five separate runs of each program.

Table 4. Comparison of pulsatile, cycle-averaged, and reduced-order model

Variable	PM	CAM	ROM
step size (s)	10^{-6}	10^{-2}	10^{-1}
V_0 (V)	29.23	27.85	27.85
V_1 (V)	64.07	64.36	64.36
V_2 (V)	9.01	9.06	9.06
CPU time (s)	13077.66	1.87	0.19

In Figure 8, we compare the dynamic response of the three models to a ramp in the resistance R_1 from 1.0 Ω to 2.0 Ω at t = 15 s.

Note that the reduced-order CAM runs 10 times faster than the CAM. The only noticeable difference in the dynamic responses is seen in the arterial voltage V_1 after the new steady state is attained. The relative error in V_1 between the ROM and the PM responses is only 2.3%, however, and therefore well within the tolerable range for the approximations made.

6. CONCLUSIONS

In this paper, we have applied circuit-averaging techniques to a simplified lumped-parameter model of the cardiovascular system. We have shown that the resultant model structure is linear and time invariant, which allows for further insight into the model structure as demonstrated by our analysis of eigenvalues and eigenvectors. The realization of a fast time-constant also led to the development of a reduced-order model using singular perturbation techniques. The cycle-averaged models allow for more generous time steps, which reduces the CPU time by a factor of 7000 for the full CAM and 70,000 for the reduced CAM, while still preserving accuracy of the simulation output. It has to be pointed out, however, that the small time step required by the PM is due to the square-wave model we have assumed for time-varying compliance; more realistic compliance variations will allow somewhat bigger time steps.

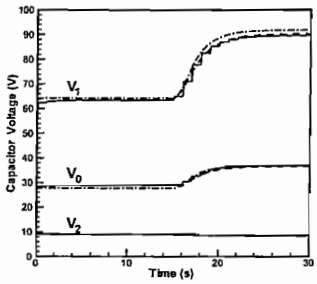

Fig. 8. Ramp in resistance R_1 at time t=15 s. PM: solid line; CAM: dashed line; ROM: dash-dotted line.

It is our main conclusion that cycle-averaging is a powerful technique to single out cardiovascular dynamics that occur on the timescale of a few cycles. Improvements in computational efficiency and insight into the model structure are gained by focusing on those components of the model that give rise to the dynamics of interest. Future work will include an improvement in the representation of V_0, more realistic compliance variation, extension to multi-chamber heart models, and addition of cardiovascular reflex mechanisms to allow for homeostatic control.

ACKNOWLEDGEMENTS

The second author is grateful for partial support from Siebel Systems. The National Aeronautics and Space Administration supported this work through the NASA Cooperative Agreement NR 9-58 with the National Space Biomedical Research Institute.

REFERENCES

Caliskan, V.A, G.C. Verghese, and A.M. Stanković (1999). Multifrequency averaging of DC/DC converters. IEEE Trans Power Electron, **14(1)**, 124-133.

Chang, J.C. (2002) Cycle-averaged models of cardiovascular dynamics. M.Eng Thesis, Department of Electrical Engineering, MIT, June.

Heldt, T., E.B. Shim, R.D. Kamm, and R.G. Mark (2002). Computational modeling of cardiovascular response to orthostatic stress. *J App Physiol*, **92**, 1239-1254.

Sunagawa, K. and K. Sagawa (1982). Models of ventricular contraction based on time-varying elastance. *Crit Rev Biomed Eng*, **7(3)**, 193-228.

Verghese, G.C. (1996). Dynamic Modeling and Control in Power Electronics In: *The Control Handbook*, (W.S. Levine, Ed.), pp. 1413-1424. IEEE Press, Boca Raton.